



Evaluation of the effects of thymoquinone on fracture healing in experimental bone fractures in rats

Duygu İlke Yıldırım, MD¹, Ahmet Yıldırım, MD², Mehmet Sedat Durmaz, MD³, Fikret Akyürek, MD⁴, Nejat Ünlükal, MD⁵, Seda Şimşek, PhD⁵, Serhat Ayan, DVM⁶

¹Department of Family Medicine, Selçuk University Faculty of Medicine, Konya, Türkiye

²Department of Orthopedics and Traumatology, Konya Health Application and Research Center, University of Health Sciences, Konya, Türkiye

³Department of Radiology, Selçuk University Faculty of Medicine, Konya, Türkiye

⁴Department of Biochemistry, Selçuk University Faculty of Medicine, Konya, Türkiye

⁵Department of Histology and Embryology, Selçuk University Faculty of Medicine, Konya, Türkiye

⁶Department of Microbiology, Faculty of Veterinary Medicine, Selçuk University, Konya, Türkiye

A bone fracture occurs when there is a complete or partial disruption of the bone's anatomical structure. Pathological fractures, often caused by metastasis from bone tumors, are increasingly common. Additionally, fractures from occupational or traffic accidents result in significant disability and economic burden. As a result, fracture healing remains a critical area of research for both scientists and physicians. Healing is a complex, regulated process influenced by various factors, and studies indicate that 5 to 10% of fractures fail to heal properly, leading to a reduced quality of life.^[1,2]

Thymoquinone (TQ) (C₁₀H₁₂O₂, 2-isopropyl-5-methyl-1,4-benzoquinone), the primary bioactive

Received: April 14, 2025

Accepted: July 20, 2025

Published online: September 12, 2025

Correspondence: Duygu İlke Yıldırım, MD. Selçuk Üniversitesi Tıp Fakültesi, Aile Hekimliği Anabilim Dalı, 42130 Selçuklu, Konya, Türkiye.

E-mail: azrailla@hotmail.com

Doi: 10.52312/jdrs.2026.2325

Citation: İlke Yıldırım D, Yıldırım A, Durmaz MS, Akyürek F, Ünlükal N, Şimşek S, et al. Evaluation of the effects of thymoquinone on fracture healing in experimental bone fractures in rats. Jt Dis Relat Surg 2026;37(1):117-130. doi: 10.52312/jdrs.2026.2325.

©2026 All right reserved by the Turkish Joint Diseases Foundation

This is an open access article under the terms of the Creative Commons Attribution-NonCommercial License, which permits use, distribution and reproduction in any medium, provided the original work is properly cited and is not used for commercial purposes (<http://creativecommons.org/licenses/by-nc/4.0/>).

ABSTRACT

Objectives: This study aims to investigate whether thymoquinone (TQ) accelerates fracture healing and modulates inflammatory and regenerative markers in a rat model.

Materials and methods: Forty-five male Wistar-Albino rats were randomly divided into seven groups and administered intraperitoneal doses of TQ. A femur fracture was surgically induced, and healing was assessed through radiological, histological, and biochemical analyses. The study included seven groups: a sham-operated control (Group 1), untreated fracture controls at two and four weeks (Groups 2 and 5), and fracture groups treated with TQ at 2.5 or 5 mg/kg/day for two weeks (Groups 3 and 4) or four weeks (Groups 6 and 7). Fracture healing was evaluated at two time points: at the end of two weeks (Groups 1-4) and at the end of four weeks (Groups 5-7). Intraperitoneal administration was chosen to ensure accurate and consistent dosing, as oral administration could lead to variability in bioavailability and potential loss during ingestion. Radiological assessments included measuring total callus diameter, radiopacity ratios, and callus surface area using high-resolution tomography. Histological analysis involved hematoxylin-eosin and immunohistochemical staining. Biochemical analyses measured complete blood count, sedimentation rate, C-reactive protein (CRP), total protein, albumin, calcium, alkaline phosphatase (ALP) and phosphorus.

Results: Significant differences in callus diameter were observed between the high dose TQ group (Group 7) and the untreated control (Group 5), while callus area showed significant differences among Groups 5, 6 and 7, and callus surface differed significantly between Groups 3 and 6. In Group 6, total protein and calcium levels increased, while albumin and ALP were lower in Group 7. Histological findings demonstrated that TQ treatment reduced dense fibrous tissue, with initial formation of spongy structures followed by trabecular bone development, indicating enhanced bone formation. Immunohistochemical analysis showed increased interleukin (IL)-10 and proliferating cell nuclear antigen (PCNA) levels, supporting improved fracture healing in high-dose groups.

Conclusion: Thymoquinone enhanced fracture healing, particularly in the fourth-week groups, improving callus formation, biochemical markers, and histological outcomes.

Keywords: Bone healing, fractures, immunohistochemistry, rats, thymoquinone.

compound in black seed oil, comprises 18.4 to 24% of the oil. It is well-known for its potent antioxidant and anti-inflammatory properties. Over the past decade, more than 1,500 studies have explored TQ's antioxidant, anti-inflammatory, anti-diabetic, anticancer, and anti-hyperlipidemic effects. However, fewer studies have examined its effects on bone healing.^[3-6] Histopathological evaluations have shown that systemic administration of TQ can accelerate new bone formation in rat tibia models, suggesting its potential as an adjunct to expedite bone healing.^[7] Additionally, TQ from *Nigella sativa* has demonstrated antioxidant effects on bone tissue by mitigating oxidative stress induced by ferric nitrilotriacetate (FeNTA).^[8]

While various factors such as stem cells, growth factors, and hemostatic agents have been explored to enhance bone healing, no studies have yet comprehensively evaluated the effects of TQ on fracture healing through histological, radiological, and biochemical assessments. In the present study, we hypothesized that TQ could accelerate fracture healing in rats in a dose-dependent manner, as evidenced by improved radiological callus formation, histological maturation, and systemic biochemical markers. We, therefore, aimed to investigate whether TQ accelerates fracture healing and modulates inflammatory and regenerative markers in a rat model.

MATERIALS AND METHODS

Forty-five male Wistar-Albino rats supplied from Selçuk University, Faculty of Medicine, Experimental Animal Laboratory were used to minimize hormonal variations. A total of rats aged between six and eight weeks weighing 280 to 300 g were housed in clean polypropylene cages with controlled humidity, temperature ($25\pm 2^{\circ}\text{C}$), and a 12-h light/dark cycle. The animals were randomly divided into seven groups and monitored throughout the study. No water restriction was applied, and they were fed standard chow without preoperative antibiotics. Intraperitoneal (IP) feeding was performed on a daily basis by the same operator to ensure procedural consistency.^[9] The study protocol was approved by the Selçuk University Experimental Medicine Application and Research Center Animal Experiments Ethics Committee (Date: 29.02.2024, No: 2024-13). All procedures involving animals were conducted in accordance with the institutional ethical guidelines for animal research and the principles of humane care, including efforts to minimize pain and distress.

Determination of the sample size

The number of animals required to assess the significance of differences in the total callus diameter (TCD)/femur diameter (FD) ratios across seven experimental groups (Group 1 to Group 7), designed to evaluate the effects of TQ on fracture healing, was determined using the Source Equation (1,2,3) method. According to this method, the number of animals per group was calculated to be 4, based on the formula $20/7+1=4$. However, to account for potential animal losses during the study, it was decided to include six animals in Groups 1-4 and seven animals in Groups 5-7, considering the anticipated higher loss rate due to the longer duration of the study.^[10,11] A total of 45 animals were included in the study.

Dose determination and preparation of TQ

Thymoquinone (15039, Cayman Chemical, MI, USA) was dissolved in ethanol at 16 mg/mL, then diluted with distilled water and administered IP to Group 3 and Group 6 at 2.5 mg/kg/day, and to Group 4 and Group 7 at 5 mg/kg/day. Doses were prepared daily in the dark to protect from light, based on previous studies.^[12,13]

Procurement of TQ

The study used TQ, which was obtained from a commercially available company (Kurul Laboratory) located in Türkiye.

Study groups: it was determined as a total of seven groups.^[14]

1. Sham group (n=6, G1): Only surgical exposure of the femur was performed without fracture induction or treatment.
2. Fracture control - 2 Weeks (n=6, G2): Femoral fracture induced; no treatment administered.
3. TQ 2.5 mg/kg - 2 Weeks (n=6, G3): Following fracture, 2.5 mg/kg/day TQ administered for two weeks.
4. TQ 5 mg/kg - 2 Weeks (n=6, G4): Following fracture, 5 mg/kg/day TQ administered for two weeks.
5. Fracture control - 4 Weeks (n=7, G5): Femoral fracture induced; no treatment administered.
6. TQ 2.5 mg/kg - 4 Weeks (n=7, G6): Following fracture, 2.5 mg/kg/day TQ administered for four weeks.
7. TQ 5 mg/kg - 4 Weeks (n=7, G7): Following fracture, 5 mg/kg/day TQ administered for four weeks.

The effects of TQ were observed during the second and fourth weeks, corresponding with significant fracture healing changes. Blood samples were taken intracardially under anesthesia. Analyzed parameters included complete blood count, sedimentation, C-reactive protein (CRP), total protein, albumin, calcium, alkaline phosphatase (ALP), and phosphorus. Group sizes were based on literature, considering potential deaths from fractures. After sacrifice, left femurs were cleaned, preserving callus, and examined radiologically and histologically. Animal care adhered to the institutional Experimental Medicine Center guidelines.

Surgical technique

After preparation, each rat was weighed to determine the appropriate anesthetic dose. Ketamine (50 mg/kg) and xylazine (10 mg/kg) were administered via the IP route. The left femur area was shaved, cleaned with povidone-iodine, and a 3-cm incision was made. The vastus lateralis muscle was retracted to expose the femur. Bone fragments were stabilized, and a 3-mm drill created a 2-mm deep bone defect, followed by sterile saline perfusion. Subcutaneous tissues were sutured, and intramedullary fixation was achieved using a 1-mm Kirschner wire (K-wire). The skin was, then, closed with 2-0 silk sutures, and rats received paracetamol (200 mg/kg) in drinking water for postoperative pain relief.

Radiological analysis

After sacrifice, the left femurs were removed and soft tissues cleaned to preserve the callus. Femurs were evaluated using conventional thin-section tomography, with each rat numbered and groups displayed in sequence. The intramedullary K-wires did not interfere with imaging, so they were not removed. Total callus diameter, low radiopacity bone (LRB), high radiopacity bone (HRB), callus surface (CS), and FDs were measured. All TCD, LRB, HRB, and FDs were measured in axial sections, while CS was measured in coronal sections, using the Radiant Dicom Viewer program (Medixant, Poznań, Poland) to calculate measurements in square millimeters.

Histological analysis

The excised tissues were fixed in 4% paraformaldehyde (PFA) at +4°C (fixative/tissue ratio 10:1) for 24 h. For decalcification, tissues were treated with 10% ethylenediaminetetraacetic acid (EDTA) (pH 7.2 to 7.4) and fresh PFA for

10 weeks. Tissues were, then, transferred to a 30% sucrose solution (with Na azide) for 24 h until they settled. After embedding in cryomatrix, tissues were sectioned at 4- μ m thickness using a cryostat (Thermo Shandon Cryostat 210160GB, Thermo Fisher Scientific, Waltham, MA, USA).

Histological studies

Hematoxylin & eosin (H&E) staining

The samples were treated twice with 99.9% absolute alcohol for 5 sec, rinsed with tap water, and stained with Harris hematoxylin for 2 min, followed by two 5-sec washes with tap water. After a rinse in absolute alcohol, the tissues were immersed in eosin for 1 min, washed twice with tap water, and rinsed three times with alcohol. The samples were, then, treated with xylene for 5 sec and mounted with Entellan. Fracture healing was scored for each section using the modified Lane and Sandhu histological scale, which evaluates callus tissue, cortex at the fracture line, and cancellous bone marrow.^[15]

Immunohistochemical labeling

For immunofluorescence labeling, sections were incubated at room temperature for 20 min in phosphate-buffered saline (PBS) with 5% bovine serum albumin (BSA) and 0.2% Triton X-100, then washed three times in PBS for 5 min each. After removing excess liquid, sections were blocked with protein block solution at 37°C for 30 min. The blocking solution was removed without washing. Primary antibodies (interleukin [IL]-10, IL-1 β , and proliferating cell nuclear antigen [PCNA]) were incubated at +4°C for one day. For conjugated antibodies (anti-IL-10 and anti-IL-1 β), sections were washed three times in PBS, mounted with 4',6-diamidino-2-phenylindole (DAPI)-containing mounting medium. For the non-conjugated anti-PCNA, sections were washed, incubated with goat anti-rabbit immunoglobulin G (IgG) (H+L) FITC secondary antibody for 3 h at room temperature, washed three times in PBS, and mounted with DAPI-containing mounting medium.

Anti-IL-10 and anti-IL-1 β antibody labeling

Sections were labeled with Alexa Fluor® 594-conjugated anti-IL-10 (sc-365858) and anti-IL-1 β (sc-32294) antibodies in a dark, humidified chamber. Images were captured using an Olympus BX51 trinocular fluorescence microscope (Olympus Corporation, Tokyo, Japan) at \times 40 magnification, with four random fields recorded for each sample

via a DP72 camera. Field validation was done at $\times 4$, $\times 10$, $\times 20$, and $\times 40$ magnifications using DAPI staining. The proportion of IL-10 and IL-1 β labeled areas to the total area was analyzed using ImageJ software (ImageJ version 1.54f, National Institutes of Health, Bethesda, MD, USA).

Anti-PCNA antibody labeling

Sections were labeled with Santa Cruz[®] Anti-PCNA Antibody (sc-25280) at 200 $\mu\text{g}/\text{mL}$ in a dark, humidified chamber. Images were captured at $\times 40$ magnification using an Olympus BX51 microscope (Olympus Corporation, Tokyo, Japan) and DP72 camera, with four random fields per section. Field validation was done using DAPI staining at $\times 4$, $\times 10$, $\times 20$, and $\times 40$ magnifications. The ratio of PCNA-labeled nuclei to total nuclei was calculated using ImageJ software (ImageJ version 1.54f, National Institutes of Health, Bethesda, MD, USA).

Statistical analysis

Statistical analysis was performed using the R version 4.2.1 software (R Foundation for Statistical Computing, Vienna, Austria). Descriptive data were presented in mean \pm standard error of mean (SEM) or number and frequency, where applicable. One-way analysis of variance (ANOVA) was used to assess differences in radiological, biochemical, immune-histological, and histopathological parameters among groups. The Tukey honestly significant difference (HSD) test was applied for pairwise comparisons. A p value of <0.05 was considered statistically significant.

RESULTS

Table I shows the radiological, biochemical, immunohistological, and histopathological evaluations.

Radiological evaluation

After sacrificing the rats and removing the left femurs, soft tissues were carefully cleaned to preserve the callus. The femurs were evaluated using conventional thin-section tomography, with each rat individually numbered and grouped in sequence. Forty-five femurs from Groups 1-7 were used for radiological evaluation. The intramedullary K-wires were not removed as they did not interfere with CT imaging. Radiological imaging was performed using a 256-slice 2-section dual-source computed tomography (CT, Somatom Definition Flash, Siemens, Germany) with parameters: slice thickness 0.75 mm, collimation width 0.6 mm, total collimation width 38.4 mm,

table speed 30.7 mm, and spiral pitch factor 0.8. Groups 2, 5, and 7 were excluded due to improper fracture formation in one femur from each group, leaving 42 femurs for analysis. Measurements of FD at the fracture level, callus diameter, largest callus area (axial plane), and CS (coronal plane) were recorded (Figure 1).

Radiological evaluation

Measurements in mm^2 were obtained using the Radiant Dicom Viewer, with images enlarged for accuracy. Each measurement was repeated three times, and the average was used for statistical analysis.

The callus diameter in G5, G6, and G7 was significantly higher than in G2, G3, and G4, with G7 also higher than G5. Groups G5, G6, and G7 exhibited significantly greater callus diameters compared to G2, G3, and G4. Specifically, G6 showed superiority over G3, and G7 over G4 (Figure 2a). The callus area in G4, G5, G6, and G7 was significantly greater than in G2, and in G5, G6, and G7 compared to G3. G6 and G7 had a significantly larger callus area than G4, and G7 had a larger area than G5 and G6. Groups G5, G6, and G7 exhibited enhanced healing in the callus area compared to G2, G3, and G4. G6 showed a significantly greater callus area than G3, and G7 than G4 (Figure 2b). The CS area in G4, G5, G6, and G7 was significantly greater than in G2, and in G5, G6, and G7 compared to G3. G6 had a significantly larger surface area than G4. The CS area in groups G5, G6, and G7 demonstrated better healing compared to groups G2, G3, and G4. Notably, G6 exhibited a significantly greater CS area than G3 (Figure 2c). The H&E staining score was significantly higher in G5, G6, and G7 compared to G2, G3, and G4.

Biochemical evaluation

The total protein level in G6 was significantly higher than in G5, G4, G3, and G2, while G7 had lower levels than G6, G5, and G4 (Figure 3a). Albumin levels in G7 were significantly lower than in all other groups (Figure 3b). Calcium levels in G7 were significantly lower than in G6, G5, and G4, while G6 had higher levels than G5, G4, G3, G2, and G1 (Figure 3c). In addition, ALP levels in G7 were significantly lower than in all other groups, and in G6, they were lower than in G5 and G2 (Figure 3d). Phosphorus levels in G7 were significantly higher than in G5, G2, and G1 (Figure 3e).

Histological results

Immunohistochemical results

Images of immunofluorescently labelled prepreparates are shown in Figures 4, 5 and 6.

TABLE I
Radiological, biochemical, immuno-histological and histopathological assessment

	G1	G2	G3	G4	G5	G6	G7	p
	Mean±SD	Mean±SD	Mean±SD	Mean±SD	Mean±SD	Mean±SD	Mean±SD	
Radiological assessment								
Femoral diameter (aksiyal)	5.183±0.132	5.067±0.093	5.470±0.162	5.602±0.128	5.293±0.105	5.061±0.082	5.057±0.064	0.005
Total femoral + callus diameter (axial)	6.288±0.308	6.288±0.308	7.000±0.206	7.372±0.154	8.087±0.106	8.250±0.173	8.705±0.141	<0.001
Callus diameter	1.298±0.364	1.298±0.364	1.530±0.077	1.770±0.232	2.740±0.187	3.189±0.197	3.637±0.087	<0.001
The widest callus area	4.069±0.869	4.069±0.869	6.431±1.113	8.807±1.103	10.791±0.739	12.747±1.121	16.554±1.249	<0.001
Callus surface (coronal)	3.512±0.893	3.512±0.893	6.577±1.020	9.109±1.038	10.154±0.904	12.075±0.679	13.024±2.256	<0.001
Biochemical assessment								
Sedimentation	3.500±0.342	2.167±0.401	2.333±0.558	3.167±0.401	2.429±0.612	2.857±0.508	2.571±0.571	0.538
TPRO	5.483±0.095	5.650±0.128	5.500±0.103	6.083±0.095	5.557±0.078	6.500±0.118	5.443±0.030	<0.001
Albumin	3.967±0.071	3.817±0.130	3.600±0.115	3.917±0.060	3.714±0.067	4.086±0.077	3.271±0.052	<0.001
Calcium	10.100±0.146	10.417±0.384	10.400±0.332	10.833±0.214	10.271±0.216	12.386±0.617	9.986±0.046	0.009
ALP	225.667±17.231	182.667±10.125	150.167±16.511	170.833±15.865	162.143±8.172	133.000±6.071	98.429±4.099	<0.001
Phosphor	7.083±0.229	8.267±0.426	8.583±0.454	8.983±0.590	8.143±0.441	11.857±1.525	9.757±0.457	0.002
Hemoglobin	14.333±0.410	14.833±0.436	13.733±0.583	13.283±0.244	14.229±0.363	14.043±0.288	14.371±0.358	0.194
Immuno-histological assessment								
IL-10	0.453±0.216	3.448±0.369	4.978±0.599	7.141±0.819	3.100±0.440	4.087±0.776	5.382±0.800	<0.001
IL1-β	1.178±0.161	8.504±1.397	8.546±0.968	6.429±0.203	5.507±0.686	6.002±0.497	3.104±0.411	<0.001
PCNA	8.378±1.634	29.153±3.898	30.572±4.528	39.807±4.555	39.013±6.000	50.768±4.394	54.987±6.011	<0.001
Histopathological assessment								
H&E staining		4.200±0.374	4.333±0.422	5.000±0.365	9.333±0.667	10.429±0.481	11.167±0.601	<0.001

SD: Standard deviation; ALP: Alkaline phosphatase; IL: Interleukin; PCNA: Proliferating cell nuclear antigen.

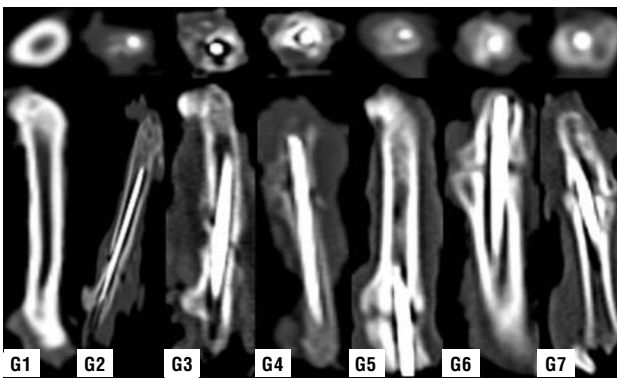


FIGURE 1. Radiological imaging results.

The immunolabeling percentages for anti-IL-10, anti-IL-1 beta, and anti-PCNA are shown in Figure 7. Significant changes were observed in the experimental groups compared to the control group. For anti-IL-10, after two weeks, G4 had significantly higher levels than G2. After four weeks, G7 was significantly higher than G5. Comparing Weeks 2 and 4, G3 was higher than G5, and G4 was higher than both G5 and G6.

Anti-IL-1 beta immunolabeling results showed significant changes in the experimental groups compared to the control. There were no differences between the two-week groups, but after four weeks, G7 was lower than G5 and G6. At both two and four weeks, G7 was significantly lower than G2, G3, and G4, G6 was lower than G3, and G5 was lower than G3.

Anti-PCNA immunolabeling showed significant differences between the control and experimental

groups, with G6 and G7 having higher levels than G2 and G3.

Histopathological results

The light microscopy images obtained by staining with H&E are presented in Figure 8. The histopathological evaluations are as follows:

- G1 (Control group): Mature bone trabeculae appeared in a regular form.
- G2: There was dense fibrous union in the fracture area. Connective tissue was predominantly observed, along with chondrocytes. Early stages of trabecular bone formation were visible.
- G3: Osteochondral union findings were observed in the fracture region. Areas of endochondral ossification consisting of connective tissue regions, chondrogenic structures, and immature trabecular bone tissue were seen.
- G4: Osteochondral union findings and connective tissue structures were visible. Areas of bone formation consisting of chondrogenic structures and immature trabecular bone tissue were present.
- G5: Areas of immature bone tissue were seen, along with areas of bone tissue. The trabeculae merged with bone marrow.
- G6: Bone union areas and new bone formation regions were observed. Reorganized trabecular bone shadows and mature bone regions were visible.

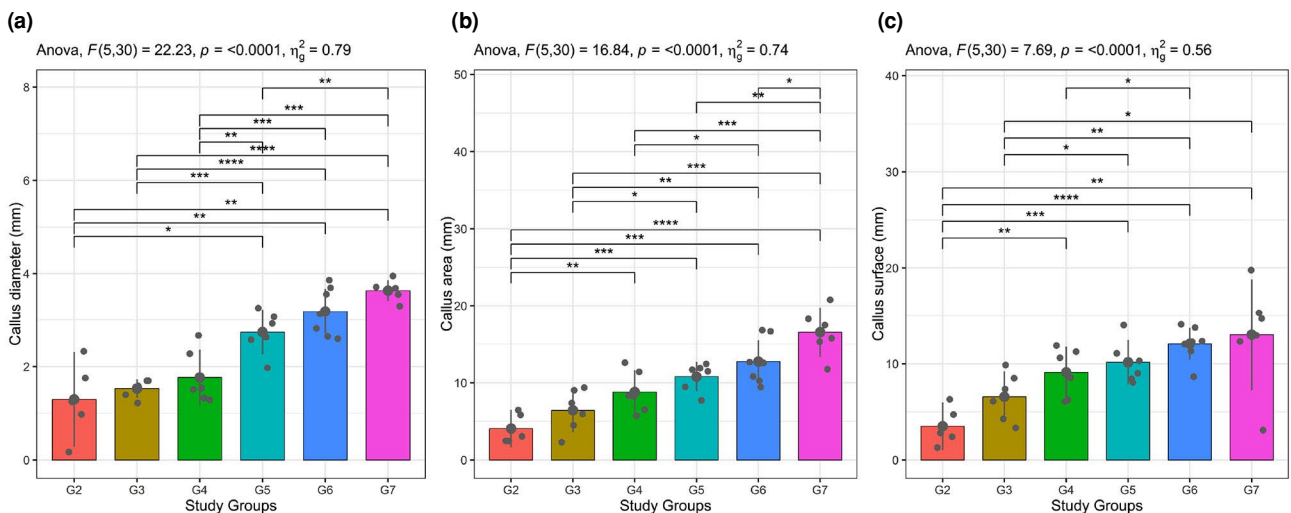


FIGURE 2. Radiological assessment of (a) callus diameter, (b) callus area, and (c) callus surface according to the groups.

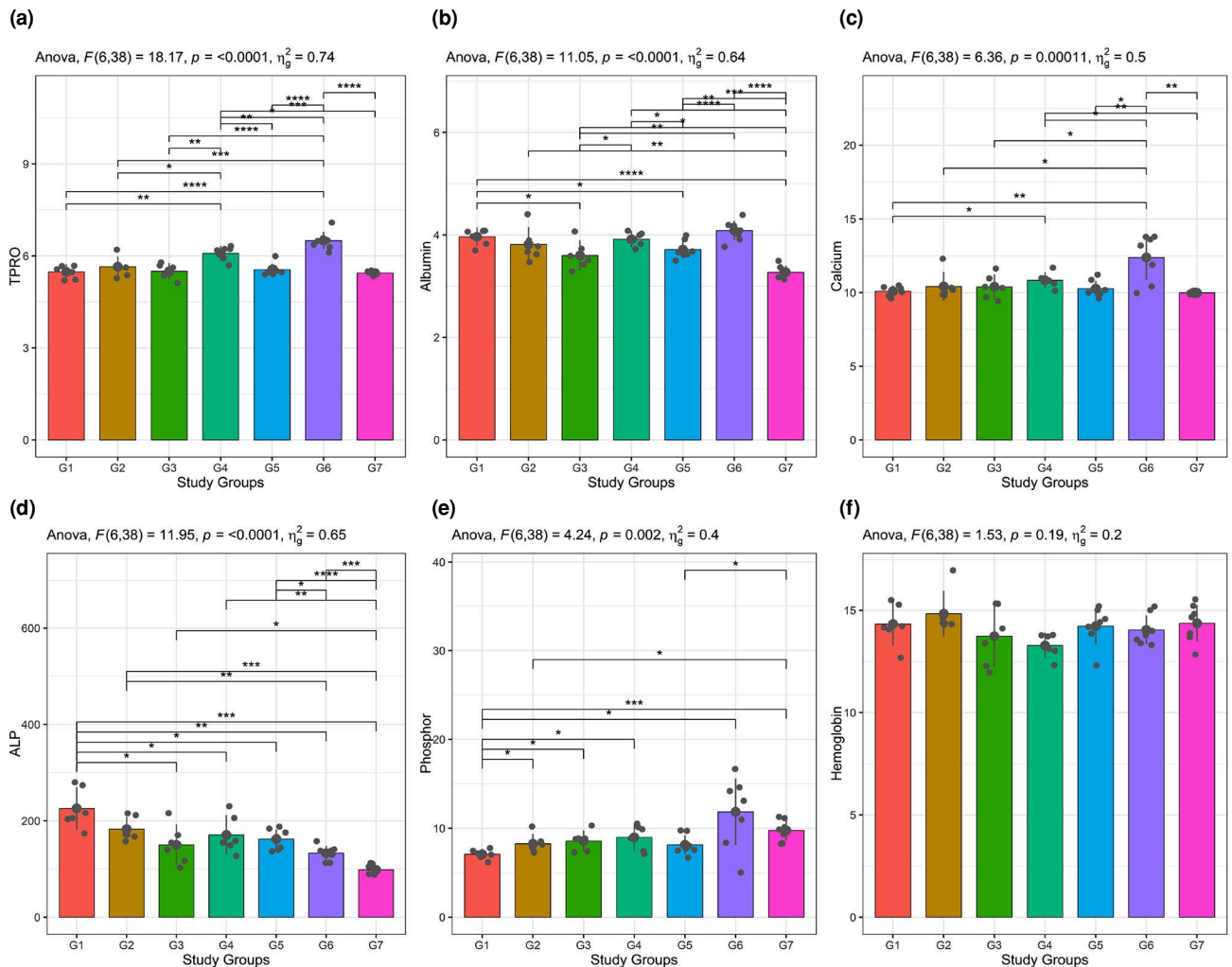


FIGURE 3. Biochemical assessment of (a) TPRO, (b) albumin, (c) calcium, (d) ALP, (e) phosphor, (f) hemoglobin according to the groups.

TPRO: Total protein; ALP: Alkaline phosphatase.

- G7: Structured bone trabeculae and bone marrow between the trabeculae were observed. (scale bar $\times 40=20 \mu\text{m}$).

Statistical analysis of H&E-stained preparations, scored according to the Lane and Sandhu criteria, is shown in Figure 9. The H&E scores in the fourth week groups were significantly higher than in the second-week groups. Additionally, the H&E scores of G6 showed significantly better healing compared to G3. The H&E scores of G7 demonstrated more significant improvement compared to G4.

DISCUSSION

In this study, the healing processes of femur fractures induced experimentally were compared across different groups through

biochemical, radiological, histopathological, and immunohistochemical evaluations. The results revealed significant differences in the bone healing process among the groups, with a particular focus on cellular and molecular changes associated with callus formation and maturation. Analysis of callus size, area, and surface showed significant differences, with Groups G5, G6, and G7 forming notably larger calluses compared to Groups G2, G3, and G4. This finding suggests that the treatments or interventions applied to these groups supported bone healing and regenerative processes.

The CT measurements revealed that callus diameter in Groups G5, G6, and G7 was significantly larger than in Groups G2, G3, and G4. Notably, the callus diameter in G7 was even greater than

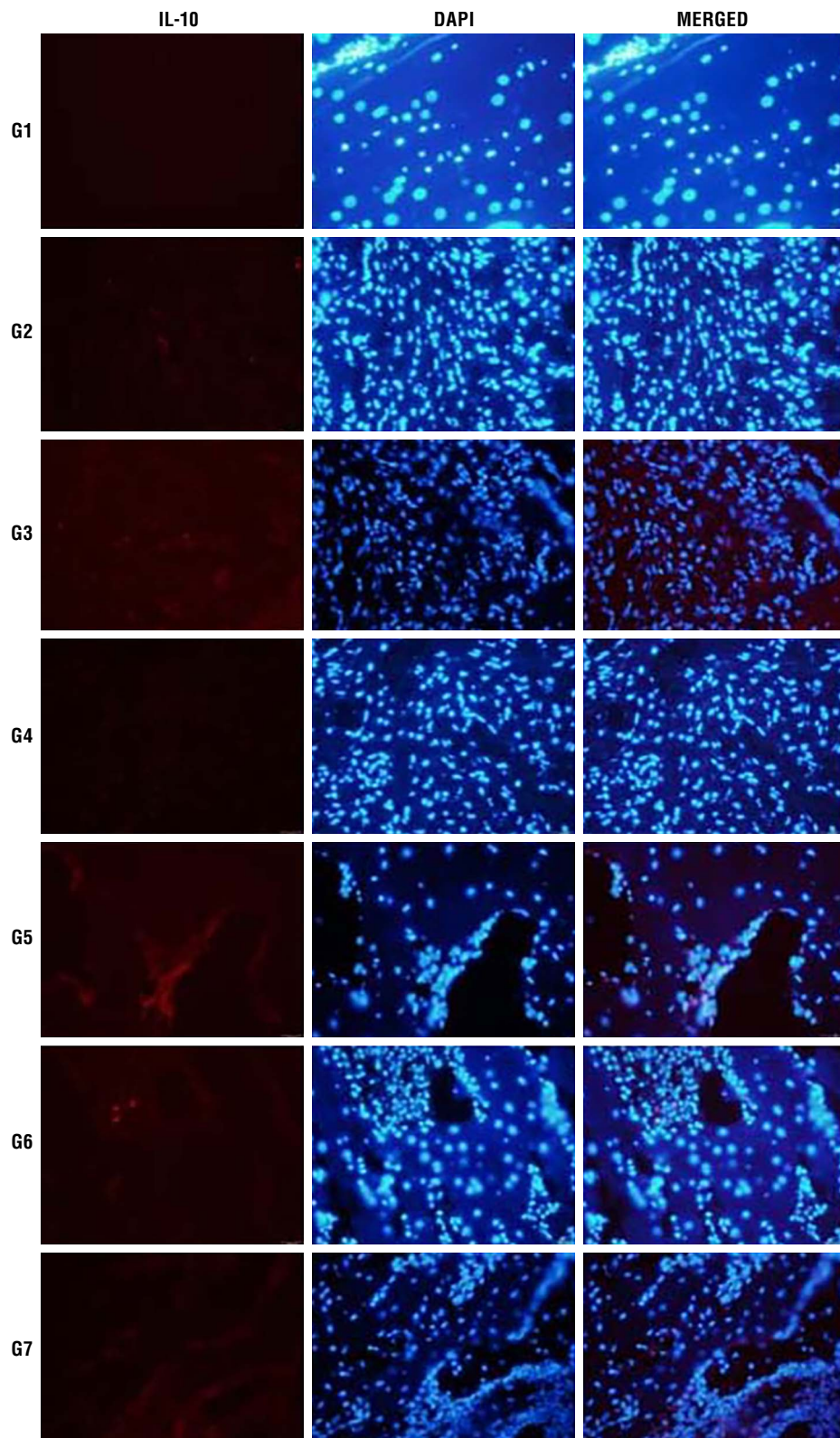


FIGURE 4. Fluorescence microscope images of bone anti-IL10 are shown under the TRITC filter (red, emission range 570 nm-620 nm) and nuclei under the DAPI filter (blue, emission range 425 nm-475 nm). Merged images were obtained by overlaying both filters. Sections were 5 μ m thick and images were taken at $\times 40$ magnification (Scale $\times 40=20 \mu$ m).
IL: Interleukin; DAPI: 4',6'-diamidino-2-phenylindole.

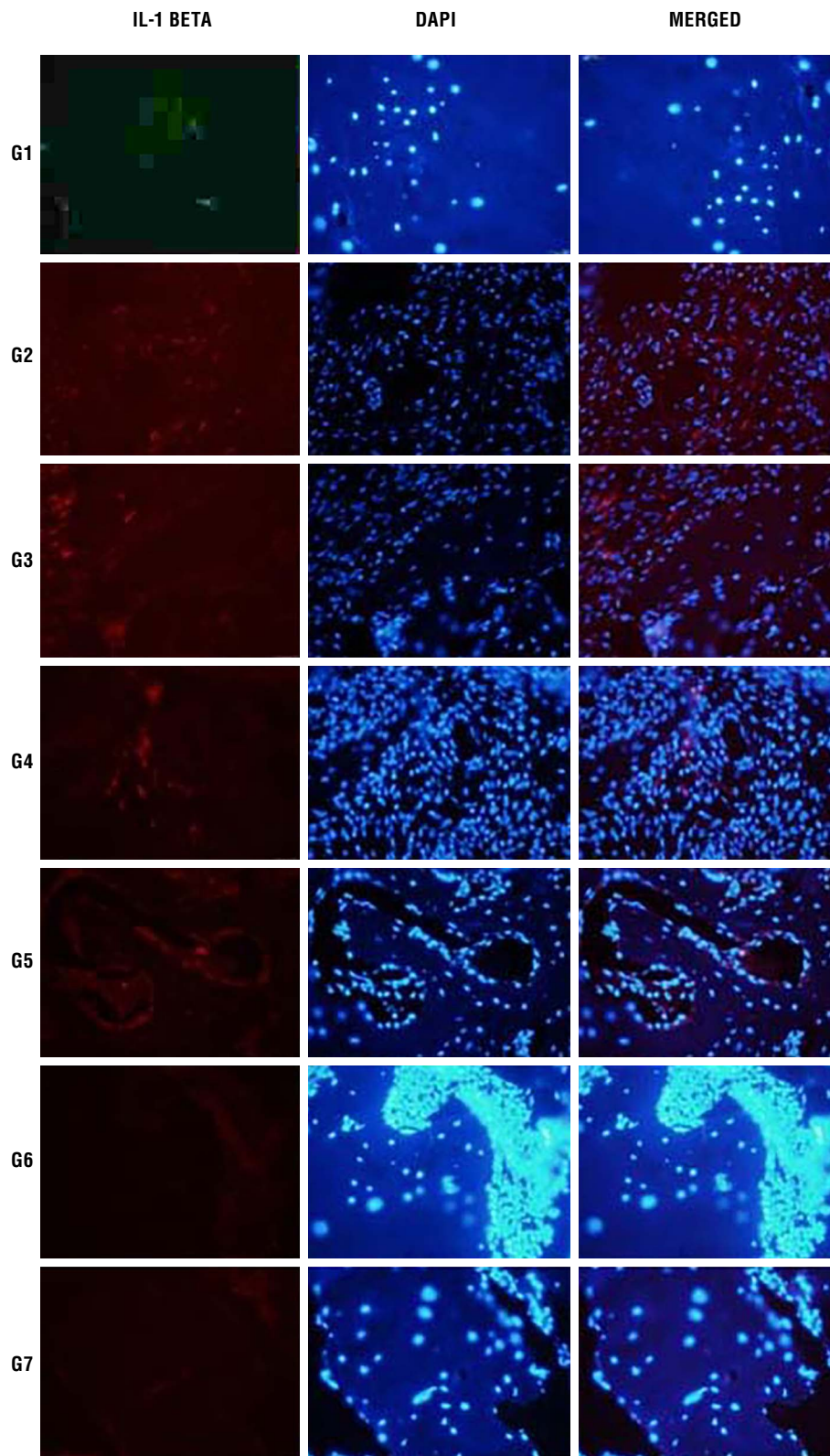


FIGURE 5. Fluorescence microscope images of bone anti-IL-1 beta are shown under the TRITC filter (red, emission range 570 nm-620 nm) and nuclei under the DAPI filter (blue, emission range 425 nm-475 nm). Merged images were obtained by overlaying both filters. Sections were 5 μ m thick, and images were taken at $\times 40$ magnification (Scale $\times 40=20 \mu$ m). IL: Interleukin; DAPI: 4',6-diamidino-2-phenylindole.

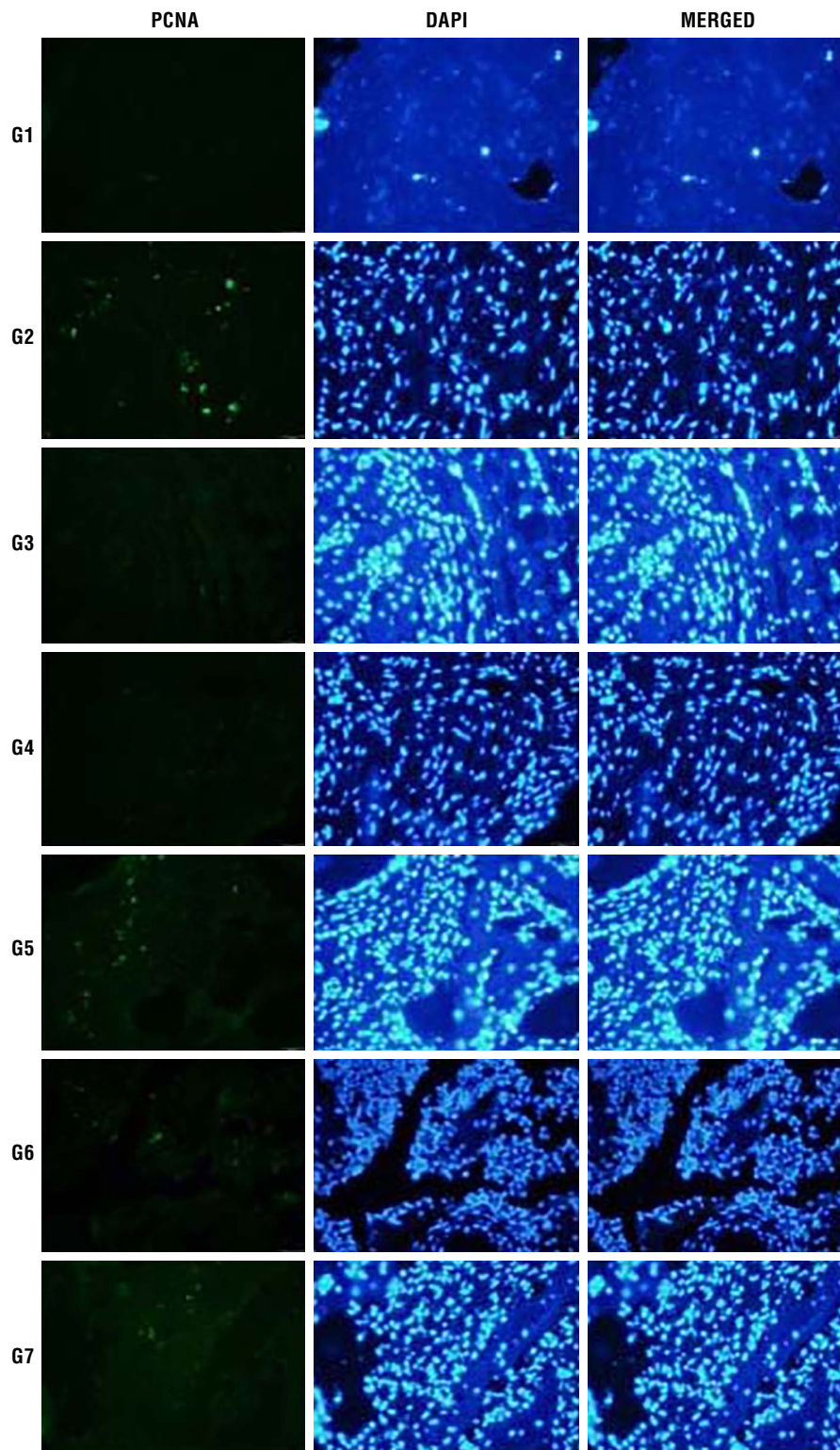


FIGURE 6. Fluorescence microscope images of bone anti-PCNA show PCNA in green under the FITC filter (500-550 nm), nuclei in blue with the DAPI filter (425-475 nm), and CdTe QDs in red with the Rhodamine filter (650-720 nm) under 710 nm excitation. Sections were 50 μm thick, and images were obtained by superimposing these filters at $\times 40$ magnification (Scale $\times 40=20 \mu\text{m}$).

PCNA: Proliferating cell nuclear antigen; DAPI: 4',6-diamidino-2-phenylindole; CdTe QDs: Cadmium telluride quantum dots.

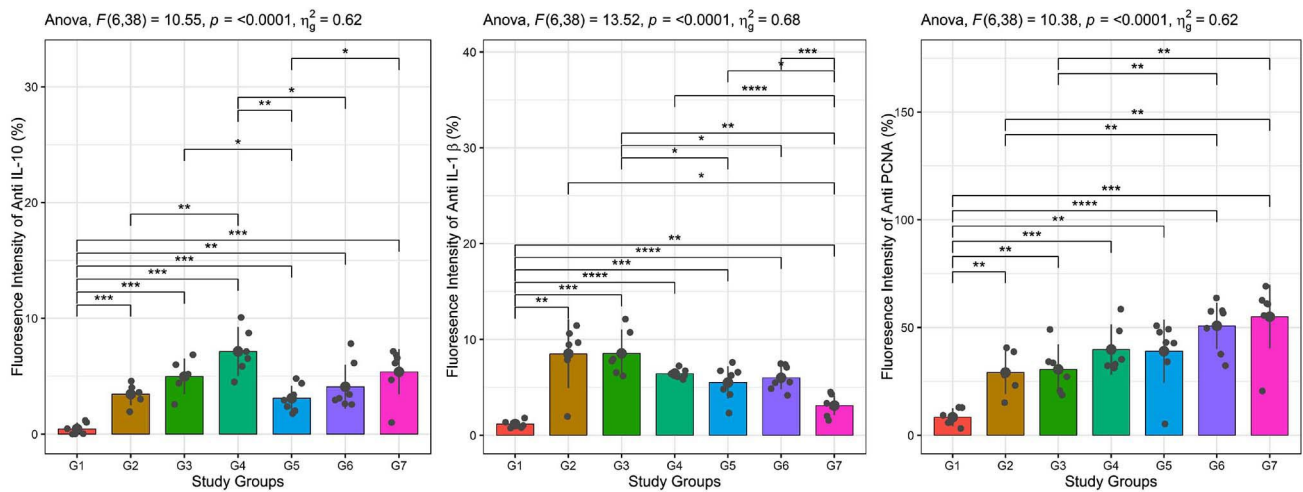


FIGURE 7. Immunohistochemistry results.
IL: Interleukin.

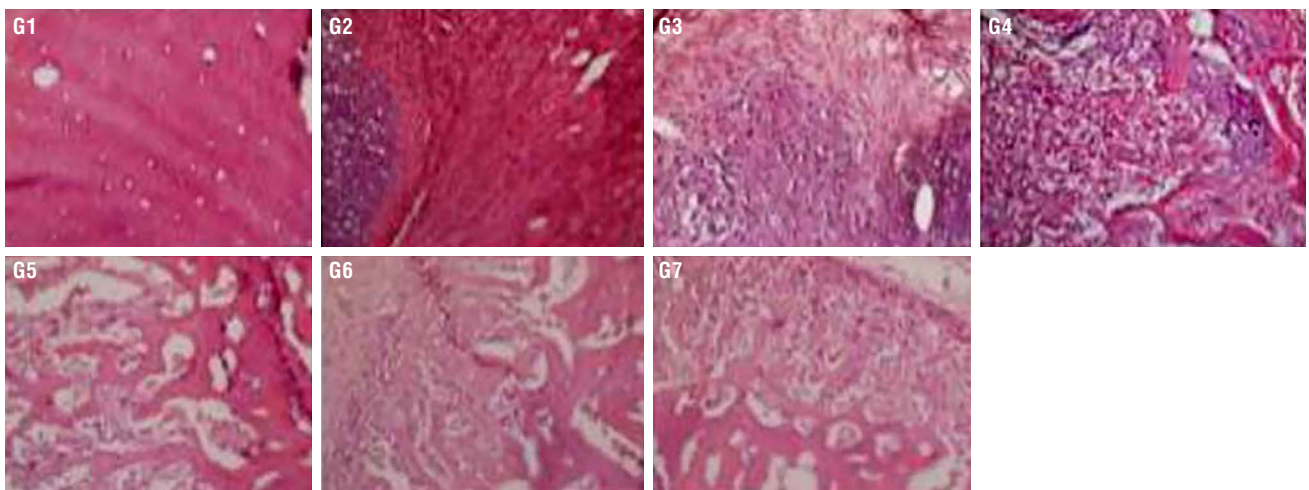


FIGURE 8. Hematoxylin and eosin (H&E) stained liver sections at $\times 40$ magnification, observed under light microscopy.

in G5, suggesting a more pronounced proliferative response in this group. Similarly, callus area measurements showed a significant increase in Groups G4, G5, G6, and G7 compared to Groups G2 and G3. G7 exhibited the largest callus area, indicating a more active bone healing process in this group. These observations highlight the importance of specific interventions in these groups, aligning with previous studies that suggest callus size and structural integrity are key indicators of effective bone healing.^[16-18]

Histopathological analysis using H&E staining showed that the four-week groups had higher healing scores compared to the second-week groups.

These findings support the idea of significant progress in bone healing over time, with a continuous regenerative response from early to late stages, in line with existing literature.^[17]

Our findings are in line with previous studies that demonstrated the beneficial effects of TQ on fracture healing. In a study conducted by Santoso et al.,^[18] orally administered TQ at a dose of 800 mg/kg enhanced osteoblast proliferation and accelerated callus formation by reducing oxidative stress through its antioxidant properties. In a study by Aliabadi et al.^[19] evaluating the effects of TQ-loaded alginate scaffolds on bone healing in a rat tibial defect model, the application of 50 μM TQ was

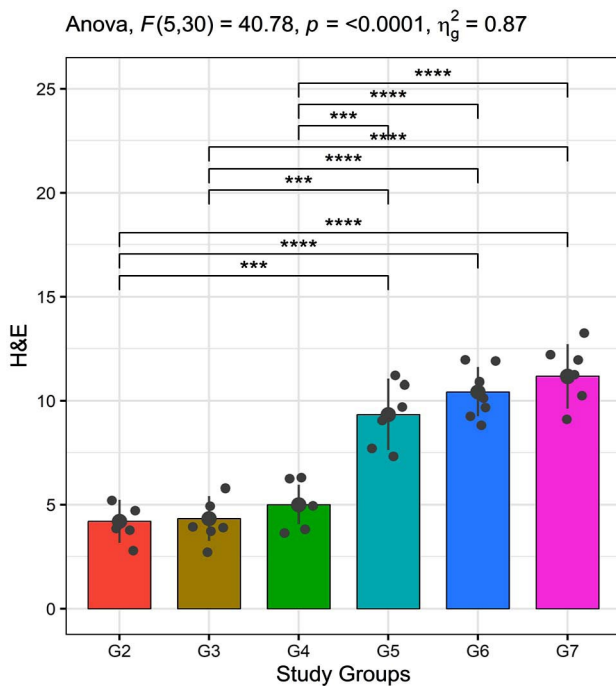


FIGURE 9. Histopathological results.

shown to increase new bone formation, osteoblast count, and capillary density. Additionally, it was suggested that TQ may accelerate bone healing through angiogenesis and BMP-2 activation. This finding suggests that the effect of TQ may plateau, and additional benefit may only be achieved at higher doses. Therefore, it highlights the need for further investigation to determine the optimal dose range of TQ and to elucidate the dose-response relationship more precisely.

Biochemical analysis revealed significantly elevated total protein levels in G6, indicative of heightened metabolic and anabolic activity associated with active bone regeneration. This aligns with the observed radiological and histological enhancements in this group, suggesting that prolonged administration of low-dose TQ may promote matrix formation and osteogenesis more effectively than higher doses. In contrast, total protein levels in G7 were lower than in G6, G5, and G4, indicating a different healing mechanism in this group. Increased total protein levels indicate enhanced tissue regeneration and metabolic activity during bone healing. Proteins, particularly collagen, play a key role in new bone matrix formation. Studies have shown that protein synthesis rises during healing, supporting bone repair. Albumin levels

were significantly lower in G7 compared to all other groups, suggesting increased albumin consumption or suppression of albumin synthesis during tissue healing. Albumin decrease during healing is linked to increased consumption due to inflammation and tissue damage or suppressed liver synthesis. This is commonly reported in trauma and postoperative recovery.^[17-22] Calcium levels in G7 were lower than in G6, G5, and G4, while G6 exhibited higher calcium levels compared to other groups. Considering the critical role of calcium in bone mineralization, the higher calcium levels in G6 suggest a more active mineralization process. Calcium is a key component of the bone matrix and essential for mineralization. High calcium levels indicate active bone formation, while calcium deficiency can delay bone healing.^[23,24]

In the current study, ALP levels were lower in G7 compared to all other groups, indicating a different bone remodeling process. The ALP is an important biochemical marker of osteoblast activity and bone mineralization. Low ALP levels may indicate reduced bone formation or a different bone remodeling process.^[25] Phosphorus levels were significantly higher in G7 compared to G5, G2, and G1, suggesting that bone metabolism in G7 follows a distinct pattern, with phosphorus potentially serving as a biomarker for changes in the bone matrix. Increased phosphorus levels are associated with changes in the bone matrix and elevated metabolic activity. Phosphorus plays an important role in bone remodeling and energy metabolism.^[26]

Immunohistochemical analyses revealed important insights into the inflammatory and regenerative processes. Anti-IL-10 staining showed that IL-10 levels in G4 were significantly higher than in G2 at two weeks, while after four weeks, G7 had higher IL-10 levels than G5, indicating a stronger anti-inflammatory response in G7. Anti-IL-1 beta staining showed lower IL-1 beta levels in G7 compared to G5 and G6 after four weeks, suggesting reduced inflammation. The G7 also showed significantly lower IL-1 beta levels at both two and four weeks compared to G2, G3, and G4, indicating rapid resolution of early inflammation and a shift to regeneration. Anti-PCNA staining revealed that proliferative activity in G6 and G7 was significantly higher than in G2 and G3, indicating ongoing cellular proliferation and key involvement in bone tissue regeneration.^[23]

Histopathological evaluation revealed the progression of bone healing across experimental

groups. Groups with more mature bone formation (e.g., G5, G6, G7) exhibited signs of trabecular bone development and remodeling, while earlier healing stages (G2, G3, G4) showed dense fibrous and cartilage-like tissue. The transition from fibrous and cartilage tissue to mature bone trabeculae reflects normal healing dynamics and highlights the importance of these groups in the fracture repair process. The H&E staining scores in Figure 5 support these findings, with G5, G6, and G7 showing significantly higher scores and more advanced healing compared to G2, G3, and G4. These results align with radiological data, indicating that larger callus formation is associated with more advanced healing stages.^[17,19,25]

Considering the limitations, this study utilized only a single animal model, which may limit the generalizability of the findings to other species or humans. The administration route was IP injection, and the effects of oral administration were not evaluated comparatively. Additionally, mechanical testing such as torsional or bending strength of the bones was not performed, which limits the assessment of functional recovery. Finally, the relatively small sample sizes and potential variability in callus measurements may affect the statistical power and reproducibility of the results.

In conclusion, this study provides strong evidence that specific therapeutic interventions in G5, G6, and G7 groups significantly enhance bone healing, as demonstrated by the improving radiological and histological outcomes in the experimental groups. Radiological and histological findings, along with immunohistochemical analyses of IL-10, IL-1 beta, and PCNA, emphasize the importance of immune and cellular responses in the fracture healing process. These findings may guide the development of future therapeutic strategies to improve fracture healing, particularly in individuals with reduced bone regeneration capacity (e.g., elderly or those with metabolic bone diseases). Further research is needed to explore the molecular mechanisms and therapeutic potential of these interventions in clinical applications.

Data Sharing Statement: The data that support the findings of this study are available from the corresponding author upon reasonable request.

Author Contributions: Idea/concept: D.İ.Y., A.Y.; Design, literature review, critical review, references and fundings, materials: D.İ.Y., A.Y., M.S.D., F.A., N.Ü., S.S., S.A.; Control/supervision, writing the article, data collection and/or processing: D.İ.Y., A.Y., M.S.D., F.A., N.Ü., S.S.; Analysis and/or interpretation: D.İ.Y., A.Y., M.S.D., N.Ü., S.S.

Conflict of Interest: The authors declared no conflicts of interest with respect to the authorship and/or publication of this article.

Funding: The authors received no financial support for the research and/or authorship of this article.

REFERENCES

- Hellwinkel JE, Miclau T 3rd, Provencher MT, Bahnney CS, Working ZM. The life of a fracture: Biologic progression, healing gone awry, and evaluation of union. *JBJS Rev* 2020;8:e1900221. doi: 10.2106/JBJS.RVW.19.00221.
- Song LM, Wang GX, Wang L. Comparison between CFR-PEEK and titanium plate for proximal humeral fracture: A meta-analysis. *Jt Dis Relat Surg* 2024;35:483-90. doi: 10.52312/jdrs.2024.1611.
- Buza JA 3rd, Einhorn T. Bone healing in 2016. *Clin Cases Miner Bone Metab* 2016;13:101-5. doi: 10.11138/ccmbm/2016.13.2.101.
- Ali Y, Akter Z, Mei Z, Zheng M, Tania M, Khan A. Thymoquinone in autoimmune diseases: Therapeutic potential and molecular mechanisms. *Biomedicine & Pharmacotherapy* 2021;134:111157. doi: 10.1016/j.biopha.2020.111157.
- Alhmied F, Alammam A, Alsultan B, Alshehri M, Pottou FH. Molecular mechanisms of thymoquinone as anticancer agent. *Comb Chem High Throughput Screen* 2021;24:1644-53. doi: 10.2174/1386207323999201027225305.
- Atta MS, Almadaly EA, El-Far AH, Saleh RM, Assar DH, Al Jaouni SK, et al. Thymoquinone defeats diabetes-induced testicular damage in rats targeting antioxidant, inflammatory and aromatase expression. *Int J Mol Sci* 2017;18:919. doi: 10.3390/ijms18050919.
- Arslan AH, Tomruk CÖ, Meydanlı EG, Özdemir İ, Çapar GD, Kütan E, et al. Histopathological evaluation of the effect of systemic thymoquinone administration on healing of bone defects in rat tibia. *Biotechnology & Biotechnological Equip* 2017;31:175-81. doi:10.1080/13102818.2016.1257925.
- Ahmad J, Albarqi HA, Ahmad MZ, Orabi MAA, Md S, Bandopadhyay R, et al. Utilization of nanotechnology to improve bone health in osteoporosis exploiting nigella sativa and its active constituent thymoquinone. *Bioengineering (Basel)* 2022;9:631. doi: 10.3390/bioengineering9110631.
- Safali S, Aydin BK, Nayman A, Ugurluoglu C. Effect of curcumin on bone healing: An experimental study in a rat model of femur fracture. *Injury* 2019;50:1915-20. doi: 10.1016/j.injury.2019.09.002.
- Mead R, Gilmour SG, Mead A. *Statistical principles for the design of experiments: applications to real experiments.* Cambridge: Cambridge University Press; 2012.
- Arifin WN, Zahiruddin WM. Sample size calculation in animal studies using resource equation approach. *Malays J Med Sci* 2017;24:101-5. doi: 10.21315/mjms2017.24.5.11.
- Malik S, Singh A, Negi P, Kapoor VK. Thymoquinone: A small molecule from nature with high therapeutic potential. *Drug Discov Today* 2021;26:2716-25. doi: 10.1016/j.drudis.2021.07.013.
- Aslam H, Shahzad M, Shabbir A, Irshad S. Immunomodulatory effect of thymoquinone on atopic dermatitis. *Mol Immunol* 2018;101:276-83. doi: 10.1016/j.molimm.2018.07.013.

14. Louw A, Diener I, Fernández-de-Las-Peñas C, Puenteadura EJ. Sham surgery in orthopedics: A systematic review of the literature. *Pain Med* 2017;18:736-50. doi: 10.1093/pm/pnw164.
15. Lane JM, Sandhu HS. Current approaches to experimental bone grafting. *Orthop Clin North Am* 1987;18:213-25.
16. Purty MK, Oraon S, Dinkar Minj S, Biswas AK, Bhusan Biswal S, Mohapatra S. Effect of *Nigella sativa* on bone mass density in albino rats. *Int J Health Clin Res* 2020;3:134-46.
17. Wang L, Tower RJ, Chandra A, Yao L, Tong W, Xiong Z, et al. Periosteal mesenchymal progenitor dysfunction and extraskeletally-derived fibrosis contribute to atrophic fracture nonunion. *J Bone Miner Res* 2019;34:520-32. doi: 10.1002/jbmr.3626.
18. Santoso AR, Huwae T, Kristianto Y, Putera MA. Effect of thymoquinone: the extract of *nigella sativa* in accelerating soft callus formation in fracture. *Int J Res Med Sci* 2019;7:4068-72. doi: 10.18203/2320-6012.ijrms20194969.
19. Aliabadi E, Farahmand MM, Talaei-Khozani T, Shahsavari-Pour S. The effects of thymoquinone loaded in alginate scaffold on bone regeneration in rabbit mandible defect. *Galen Med J* 2023;12:e3141. doi: 10.31661/gmj.v12i.3141.
20. Luo W, Wang Y, Han Q, Wang Z, Jiao J, Gong X, et al. Advanced strategies for constructing interfacial tissues of bone and tendon/ligament. *J Tissue Eng* 2022;13:20417314221144714. doi: 10.1177/20417314221144714.
21. Cardoneanu A, Rezus C, Tamba BI, Rezus E. Bone cells metabolic changes induced by ageing. *Subcell Biochem* 2023;103:13-29. doi: 10.1007/978-3-031-26576-1_2.
22. Tanrikulu S, Gönen E. Fracture healing. *J TOTBiD* 2017;16:455-75.
23. Raggatt LJ, Partridge NC. Cellular and molecular mechanisms of bone remodeling. *J Biol Chem* 2010;285:25103-8. doi: 10.1074/jbc.R109.041087.
24. Ferreira CR, Carpenter TO, Braddock DT. ENPP1 in blood and bone: Skeletal and soft tissue diseases induced by ENPP1 deficiency. *Annu Rev Pathol* 2024;19:507-40. doi: 10.1146/annurev-pathmechdis-051222-121126.
25. Sekaran S, Vimalraj S, Thangavelu L. The physiological and pathological role of tissue nonspecific alkaline phosphatase beyond mineralization. *Biomolecules* 2021;11:1564. doi: 10.3390/biom11111564.
26. Gerlinger C, Oster M, Reyer H, Polley C, Vollmar B, Muráni E, et al. Effects of excessive or restricted phosphorus and calcium intake during early life on markers of bone architecture and composition in pigs. *J Anim Physiol Anim Nutr (Berl)* 2021;105 Suppl 2:52-62. doi: 10.1111/jpn.13286.